AD-A045 143 GRUMMAN AEROSPACE CORP BETHPAGE N Y RESEARCH DEPT F/G 14/5
DIGITAL PROCESSING OF AIRCRAFT IMAGES TO EXTRACT SILHOUETTES.(U)
JUL 77 G GARDNER, J MENDELSOHN, M WOHLERS

UNCLASSIFIED RM-640 NL

1 OF 1
AD
A045143

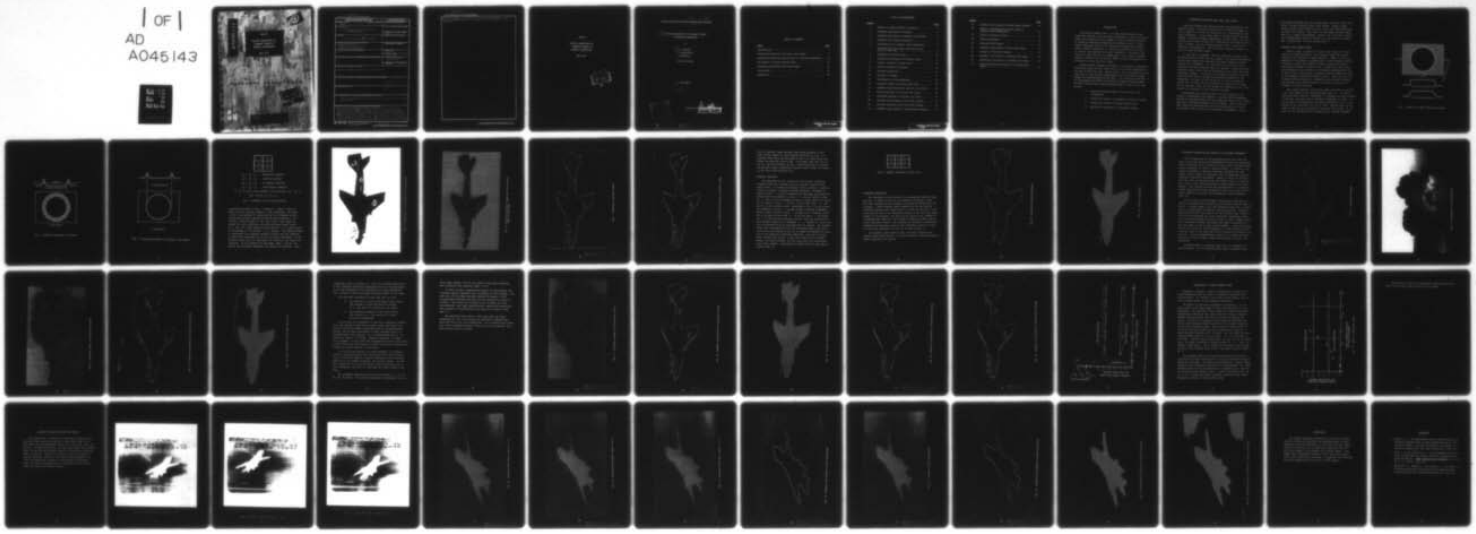

END
DATE
FILMED
11-77
DDC

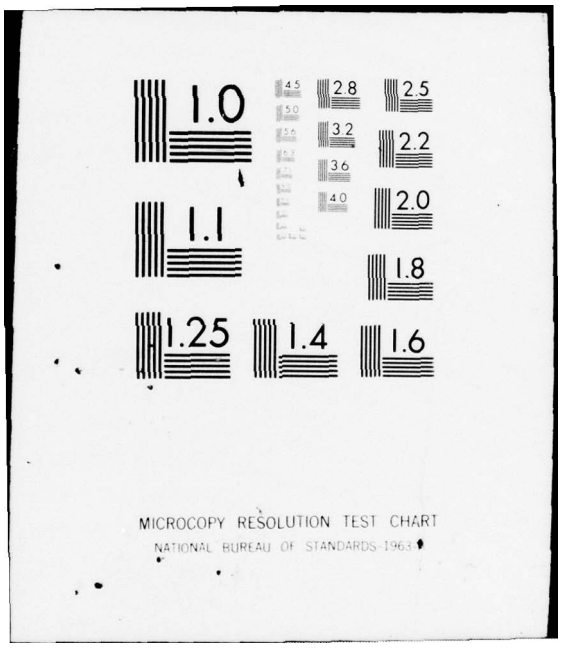
1.0
1.1
1.25
1.4
1.6
1.8
2.0
2.2
2.5
2.8
3.2
3.6
4.0
4.5
5.0
MICROCOPY RESOLUTION TEST CHART
NATIONAL BUREAU OF STANDARDS-1963-A

12

RM-640

DIGITAL PROCESSING OF AIRCRAFT IMAGES TO EXTRACT SILHOUETTES

JULY 1977

RESEARCH DEPARTMENT

GRUMMAN AEROSPACE CORPORATION
BETHPAGE, NEW YORK

UNCLASSIFIED

SECURITY CLASSIFICATION OF THIS PAGE *(When Data Entered)*

REPORT DOCUMENTATION PAGE		READ INSTRUCTIONS BEFORE COMPLETING FORM
1. REPORT NUMBER RM-640	2. GOVT ACCESSION NO.	3. RECIPIENT'S CATALOG NUMBER
4. TITLE *(and Subtitle)* Digital Processing of Aircraft Images to Extract Silhouettes		5. TYPE OF REPORT & PERIOD COVERED 6. PERFORMING ORG. REPORT NUMBER RM-640
7. AUTHOR(s) G. Gardner, J. Mendelsohn, & R. Wohlers		8. CONTRACT OR GRANT NUMBER(s)
9. PERFORMING ORGANIZATION NAME AND ADDRESS Research Department, Grumman Aerospace Corporation Bethpage, New York 11714		10. PROGRAM ELEMENT, PROJECT, TASK AREA & WORK UNIT NUMBERS
11. CONTROLLING OFFICE NAME AND ADDRESS		12. REPORT DATE July 1977 13. NUMBER OF PAGES 46
14. MONITORING AGENCY NAME & ADDRESS*(if different from Controlling Office)*		15. SECURITY CLASS. *(of this report)* Unclassified 15a. DECLASSIFICATION/DOWNGRADING SCHEDULE

16. DISTRIBUTION STATEMENT *(of this Report)*

Approved for Public Release; Distribution Unlimited

17. DISTRIBUTION STATEMENT *(of the abstract entered in Block 20, if different from Report)*

18. SUPPLEMENTARY NOTES

19. KEY WORDS *(Continue on reverse side if necessary and identify by block number)*

digital processing, image processing, aircraft silhouette, edge detection, sensor jitter

20. ABSTRACT *(Continue on reverse side if necessary and identify by block number)*

Work done at Ohio State University has resulted in the development of digital techniques to classify aircraft from visual images using moment invariants of the aircraft silhouette. Application of these techniques requires a clear silhouette and is often impossible to apply to images which contain blurring or background clutter. This memorandum describes digital image processing techniques which will allow the extraction of representative silhouettes from noisey images. These techniques include edge detection and

DD FORM 1 JAN 73 1473 EDITION OF 1 NOV 65 IS OBSOLETE
S/N 0102-014-6601

Unclassifed

SECURITY CLASSIFICATION OF THIS PAGE *(When Data Entered)*

frame averaging and are applied to visual images with background clutter and blurring due to sensor jitter. Application to FLIR images is also presented.

RM-640

DIGITAL PROCESSING OF AIRCRAFT IMAGES TO EXTRACT SILHOUETTES

JULY 1977

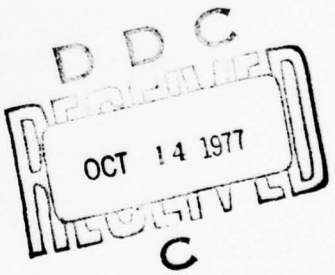

Grumman Research Department Memorandum RM-640

DIGITAL PROCESSING OF AIRCRAFT IMAGES TO EXTRACT SILHOUETTES.

by

G. Gardner,
J. Mendelsohn
M. Wohlers

System Sciences

July 1977

54 p.

Approved by: Richard A. Scheuing
Richard A. Scheuing
Director of Research

TABLE OF CONTENTS

LIST OF ILLUSTRATIONS

INTRODUCTION

Work done by Dudani (Ref. 1) at Ohio State University has shown that aircraft can be reliably identified by their silhouettes. Dudani used digitized optical images of model aircraft from which he extracted silhouette boundaries and interior points. Using moment invariants based on the silhouette boundary and interior points, Dudani constructed 14 features with which he was able to classify the aircraft with great reliability. Because of the success of this work and its significance to the field of Identification, Friend, Foe, or Neutral (IFFN) we have investigated its application to more realistic images.

Because Dudani obtained his images in a laboratory environment using clean white aircraft models with a solid black background, he was able to work with pure, binary images. This eliminated from his study many of the problems encountered in the real world imaging needed for implementation in the field. In a previous study (Ref. 2) we investigated the effect of blurring on Dudani's binary images. The work reported here further extends Dudani's work in four ways. We have

1) used real aircraft images with full gray scale illumination
2) studied the effects of background noise and clutter
3) studied the effects of sensor-induced noise
4) applied our techniques to nonoptical imagery

SILHOUETTE EXTRACTION FROM GRAY LEVEL IMAGES

With the ultimate goal being aircraft classification by silhouette moments, the first step must be to process the image in such a manner as to allow the extraction of a representative aircraft silhouette. If the image shows a strongly backlit aircraft against a uniformly brighter background, or vice versa, the silhouette can be easily extracted by thresholding the image intensity. This, in effect. was the situation Dudani used to simplify his silhouette determination. This fortuitous situation, however, is rare in actual aircraft images.

We are faced, in general, with the difficult problem of dividing the digital image into two regions. All points representing the aircraft comprise the aircraft silhouette, while all others comprise the background. Our task then is to find the closed bounding curve that separates these two regions. Since all points interior to this curve form the silhouette we call this curve the silhouette boundary. In theory, the silhouette boundary is an abstraction that lies on neither the aircraft silhouette or the background. In fact, we will obtain it as a set of digitized points each of which must lie in either one region or the other. For our purposes, then, we will define the silhouette as all those points on or interior to the silhouette boundary.

Determining the silhouette points is then reduced to the problem of determining its boundary. Features that discriminate between the aircraft region and the background region will be those that show a difference between the two regions. With a view towards real-time implementation with high reliability, we need a discriminant that is simple and consistently dependable. Since

the imaging equipment and data we had access to had no color capability, we were limited to gray level images. Texture offers little promise since aircraft as well as sky and cloud backgrounds all tend to be smooth. This leaves us with image intensity (gray level) as a region discriminant. Indeed, one of the most reliable and straightforward boundary detectors is the intensity gradient and, in particular, its local maxima (Ref. 2).

GRADIENT LOCAL MAXIMA METHOD

Figure 1 shows an example of a gray level image of a bright circle on a dark background. Also shown are ideal and typical measured cross sections of image intensity. Figure 2 shows the magnitude of the intensity gradient and a crude boundary comprised of points at which this gradient exceeds a defined threshold. A much sharper boundary is shown on Fig. 3 where only those points corresponding to local maxima of the gradient magnitude are used. In other words, those points of maximum intensity difference serve as the sharpest discriminant between regions. Note also that the standard gradient boundary is dependent on the threshold whereas the gradient local maxima boundary is constant as long as the threshold is below the peaks.

This simple gradient local maxima (GLM) technique was applied to the test images in the following manner (Fig. 4). In each of four directions (vertical, horizontal, up diagonal and down diagonal), a two-point, absolute value of intensity difference is taken. If any of these four directional derivative magnitudes is not a local maximum in its direction it is set to zero. The GLM value at the point is then set at the maximum of the final four values. An example of this procedure and a comparison with standard gradient

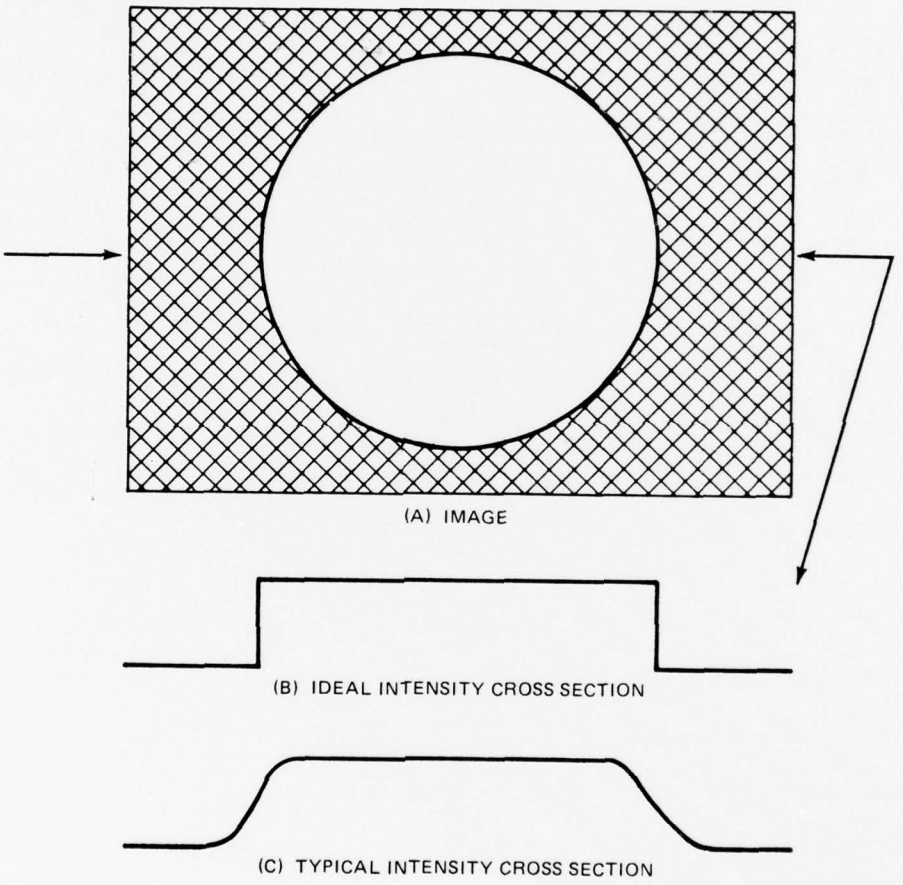

Fig. 1 Example of Image Intensity Variation

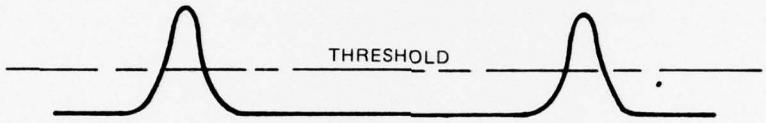

(A) INTENSITY GRADIENT MAGNITUDE

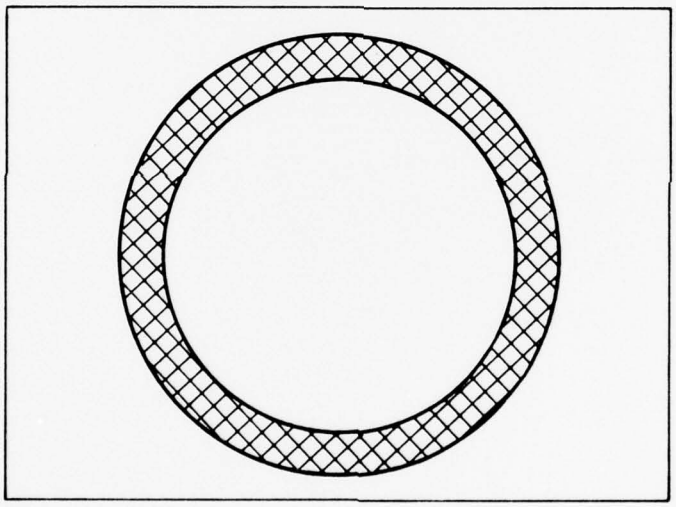

(B) OBJECT BOUNDARY

Fig. 2 Boundary Determined by Gradient

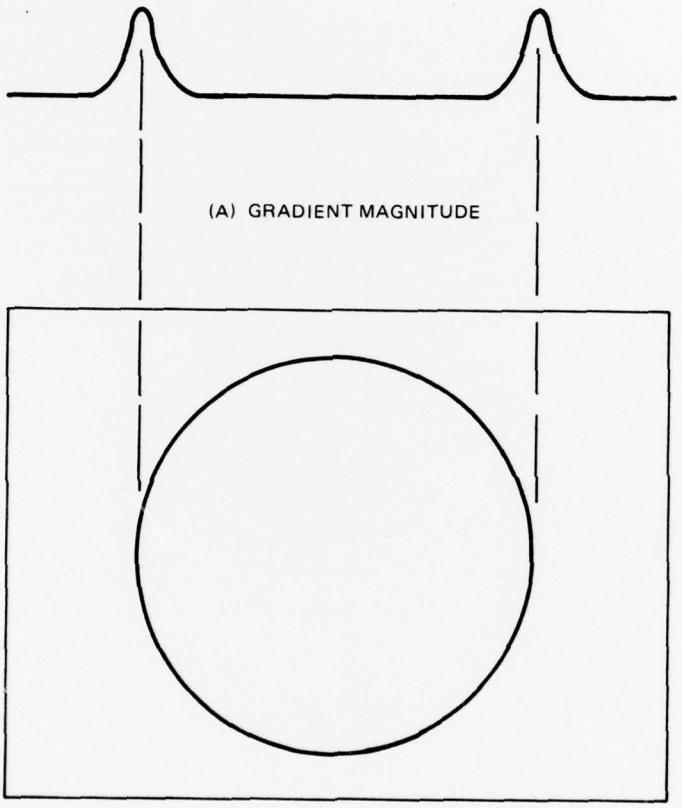

Fig. 3 Boundary Determined by Gradient Local Maxima

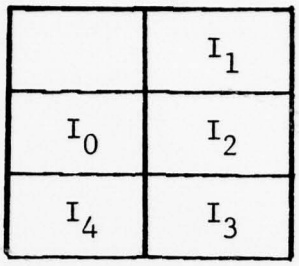

$G_1 = I_0 - I_2$ Horizontal Gradient

$G_2 = I_0 - I_4$ Vertical Gradient

$G_3 = I_0 - I_1$ Up Diagonal Gradient

$G_4 = I_0 - I_3$ Down Diagonal Gradient

If G_i is not a local maximum in its direction, set $G_i = 0$

$$GLM = \max\{G_1, G_2, G_3, G_4\}$$

Fig. 4 Gradient Local Maxima Algorithm

processing are shown in Figs. 5 through 8. Figure 5 shows an image of an A-6 aircraft against a clean background. The image in Fig. 6 was obtained by digitizing the A-6 photograph using a Spatial Data Systems Computer Eye System which produced a 512 column by 480 row image of 256 gray levels. This image was reduced (to save computation time and facilitate image output) to a 128 x 120 point image by replacing each 4 x 4 point square by the average of its interior 2 x 2 squares. The digitized image is represented on a computer terminal printout with the intensity at each point represented by one of ten printed characters. In the intensity image (Fig. 6), the higher the intensity, the darker the character. In the gradient and GLM images (Figs. 7 and 8), the greater the derivative magnitude, the darker the character. Note

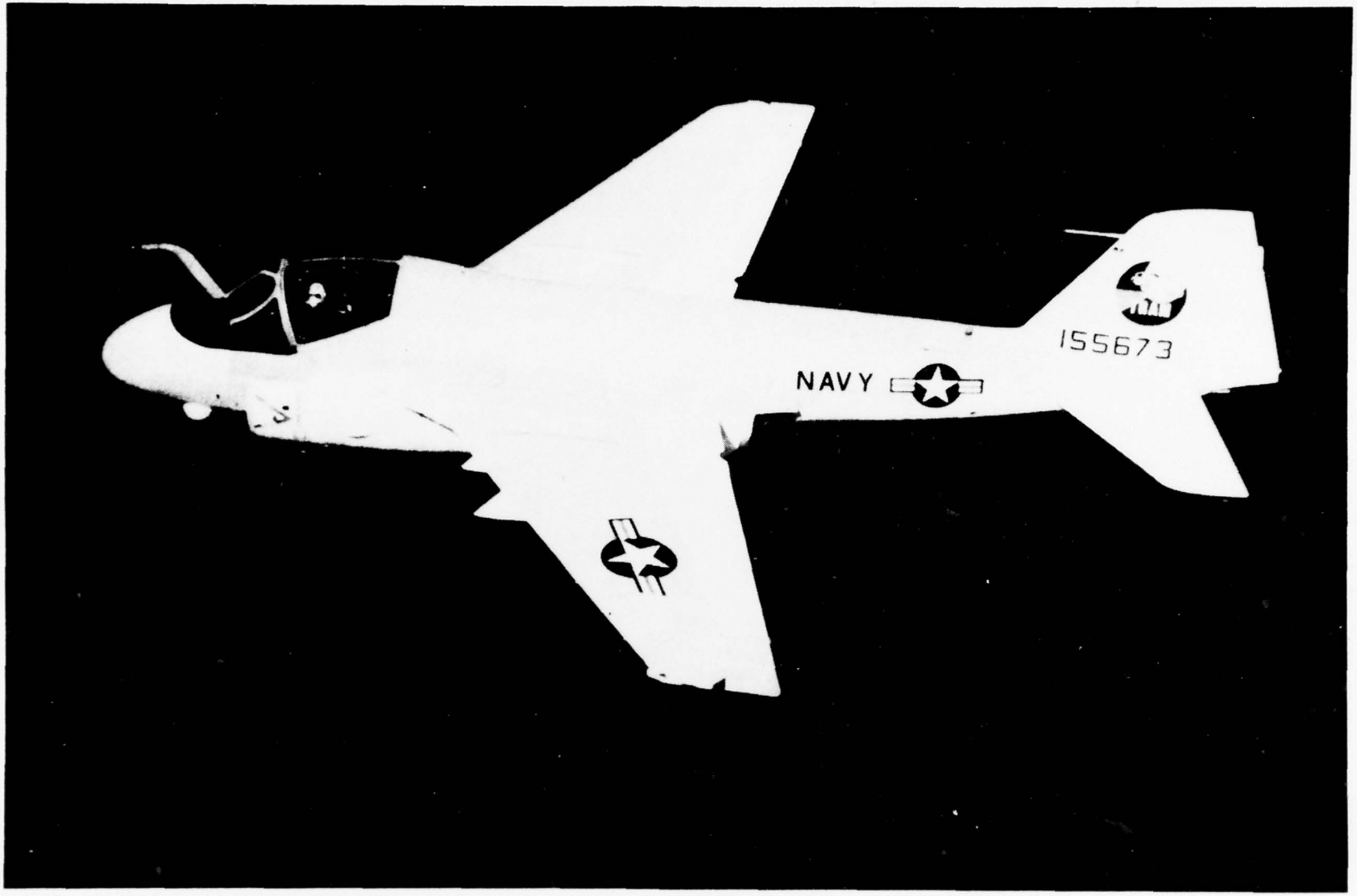

Fig. 5 Photograph of A-6 Against Clear Background

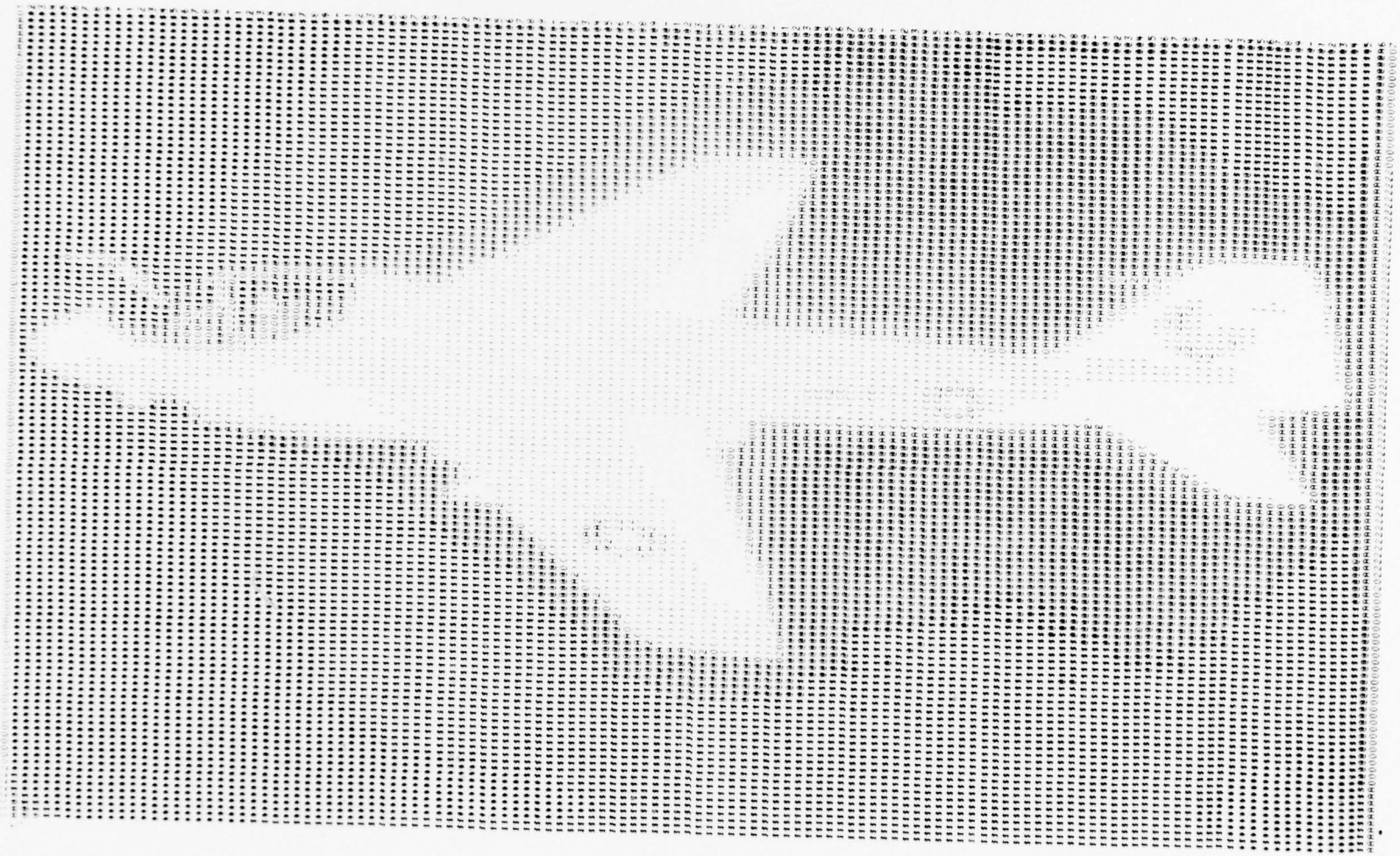

Fig. 6 Digitized Aircraft Image (Ten Gray Levels)
(A-6 in Clear Sky)

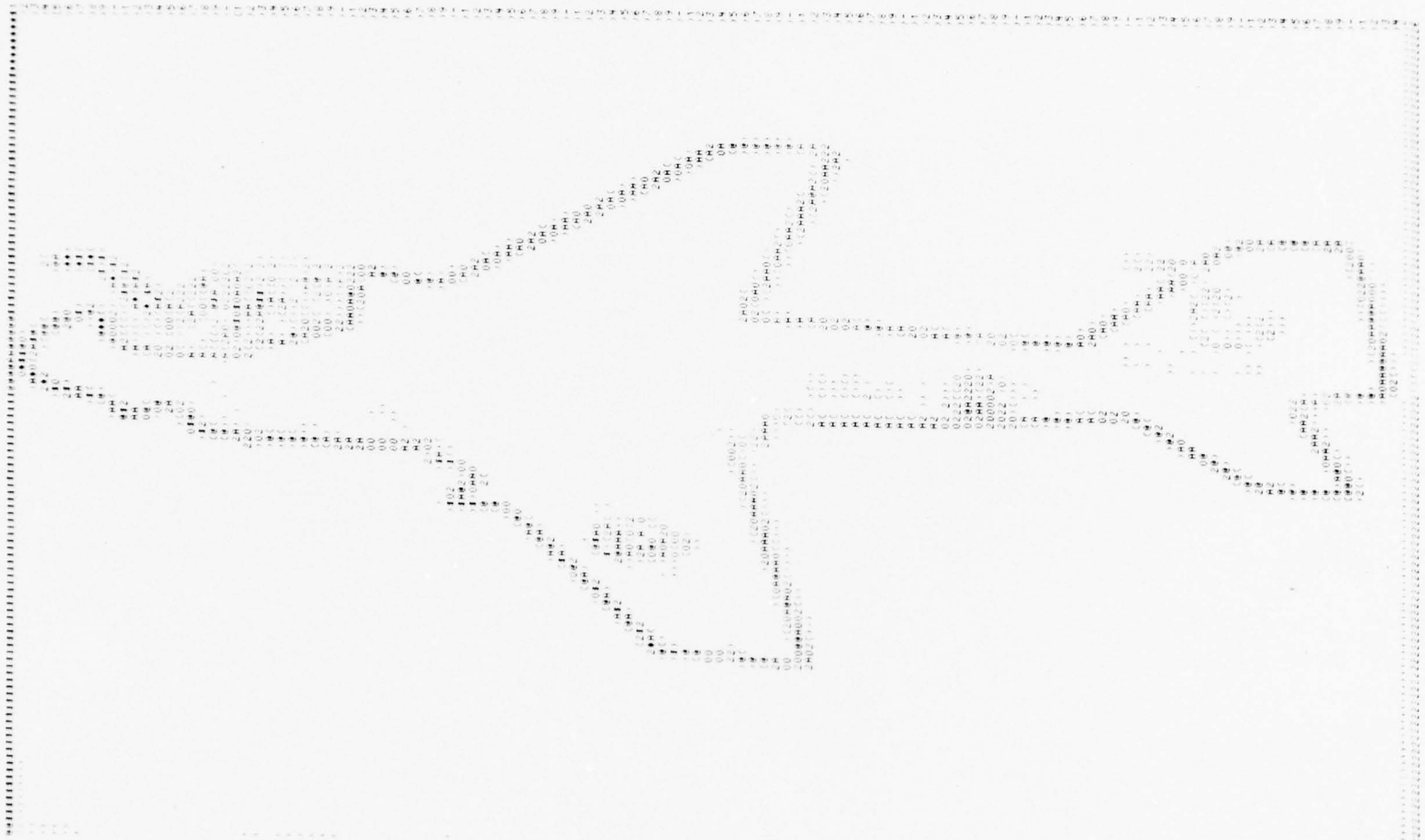

Fig. 7 Gradient of Aircraft Image

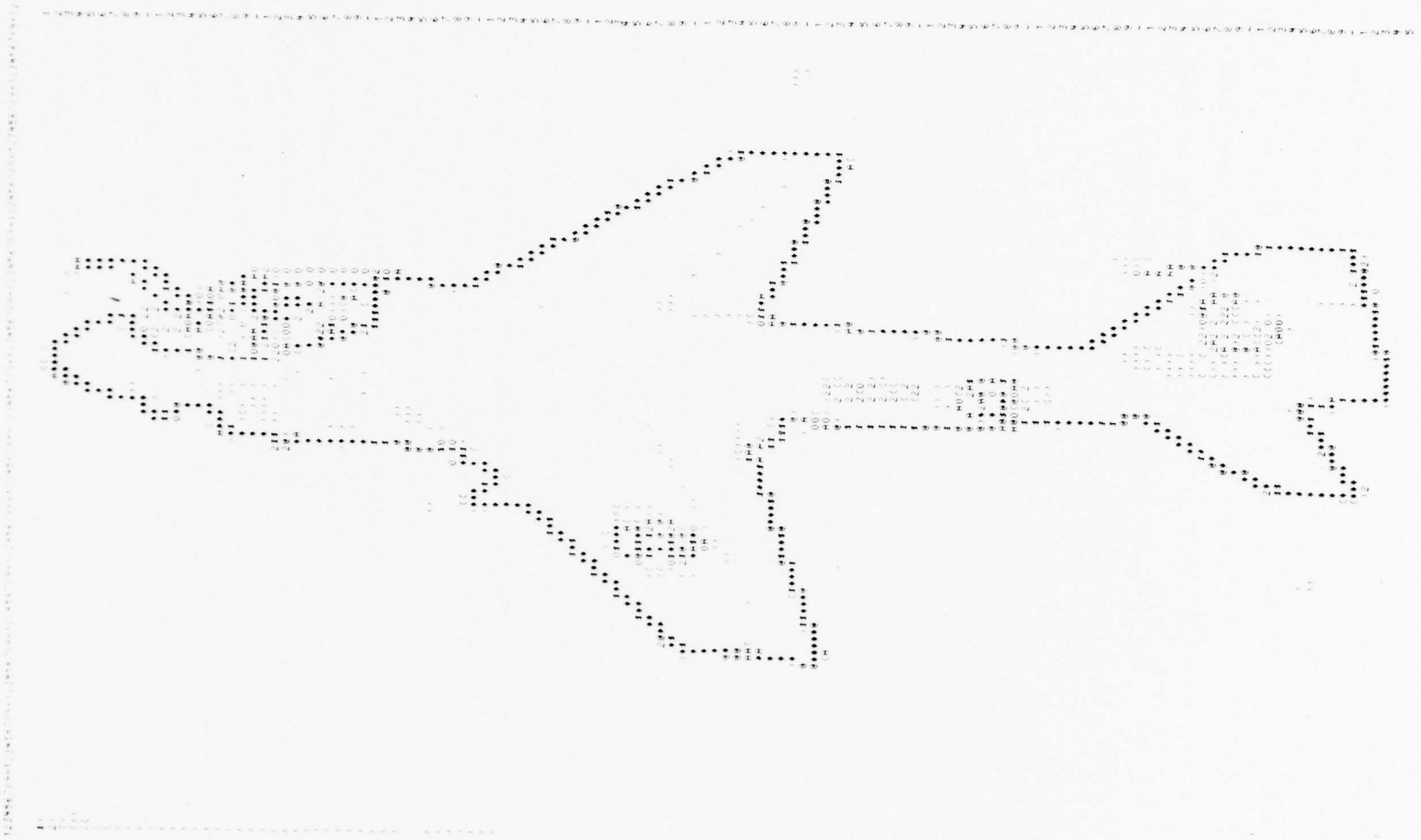

Fig. 8 Gradient Local Maxima of Aircraft Image

that the gradient image (maximum directional gradient at each point without regard to local maximum criterion) in Fig. 7 is somewhat fuzzy while the GLM image in Fig. 8 is quite sharp even though the threshold used in Fig. 7 was higher than that used in Fig. 8. Had the threshold in Fig. 7 been raised more to sharpen the gradient image, significant boundary points (below the snorkel on the nose) would have been lost.

BOUNDARY FOLLOWING

The GLM image in Fig. 8 gives all the aircraft silhouette boundary points but includes points of interior detail and exterior noise. To isolate the boundary curve we employ a modified version of Dudani's boundary following algorithm, explained in detail in Ref. 1. First we threshold the GLM image and assign all values above the threshold a value of 1 and all others a value of 0. Next we scan the image from left to right and top to bottom until a point of value 1 is hit. We call this point "x" and save it as the starting point. Referring to Fig. 9, we now search the neighbors of point x counterclockwise starting at Neighbor 2. When we reach a point of value 1 we mark it as a boundary point and it becomes the new point x. If the new point x was Neighbor i of the previous boundary point we start the counterclockwise neighbor search at its Neighbor i - 2 (Module 8). This last step is repeated until the starting point is reached. Any boundary point that is encountered twice (by returning along a thin point such as the tail antenna in Fig. 8) is marked accordingly for later use in the silhouette completion algorithm. Note that if small noise blotches are circled, a test can be made on the boundary length, the points deleted, and the scan search for the boundary start point resumed. The boundary isolated from the GLM image is shown in Fig. 10.

0	7	6
1	x	5
2	3	4

Fig. 9 Dudani's Boundary Follower Code

SILHOUETTE COMPLETION

The silhouette can be filled in by scanning the boundary image from left to right on each row and marking as silhouette points all those starting with odd boundary crossings and ending with even crossings. (Those boundary points marked twice in the boundary isolation algorithm are counted twice, as both odd and even.) Some holes will be left in the silhouette because of the scan line being tangent to the boundary, but these can be filled in by scanning in a perpendicular direction, and filling in between boundary and interior silhouette points. The procedure is repeated in alternating perpendicular directions until no new silhouette points are found. The resulting silhouette for the A-6 is shown in Fig. 11.

The boundary points shown in Fig. 10 and the complete silhouette points shown in Fig. 11 can now be used to calculate Dudani's moment invariants for the A-6.

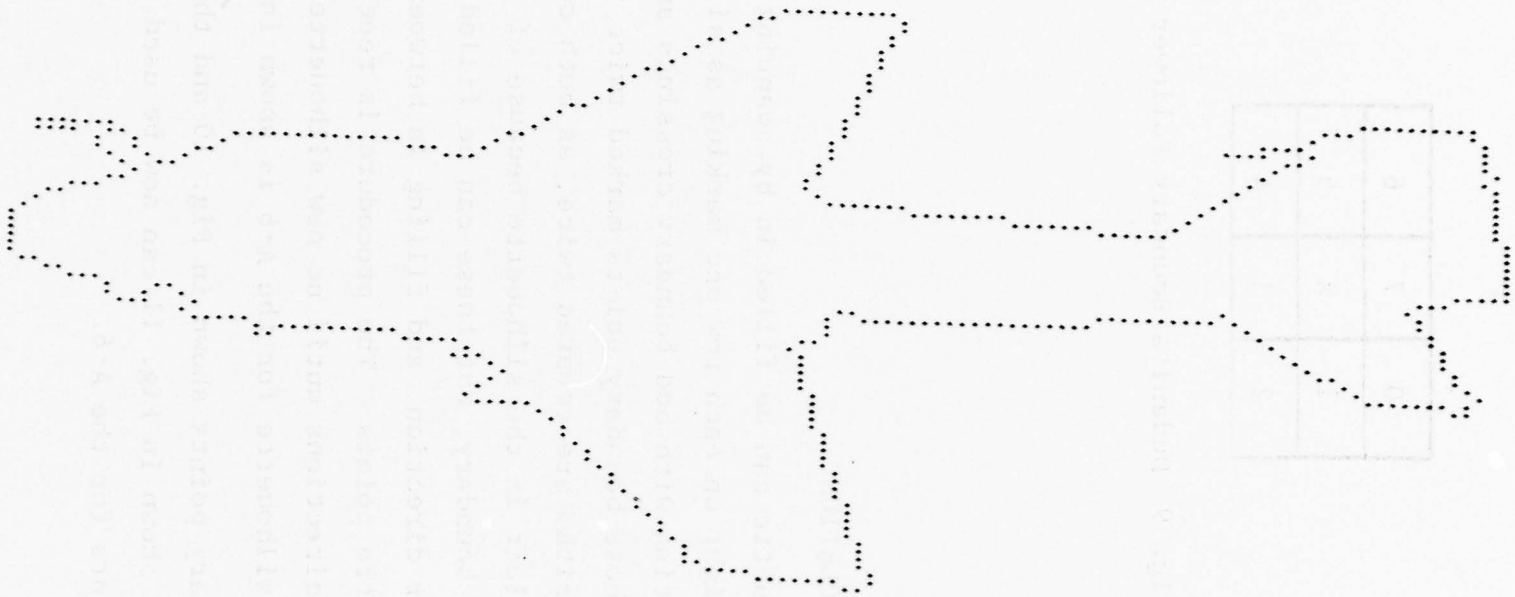

Fig. 10 Aircraft Silhouette Boundary

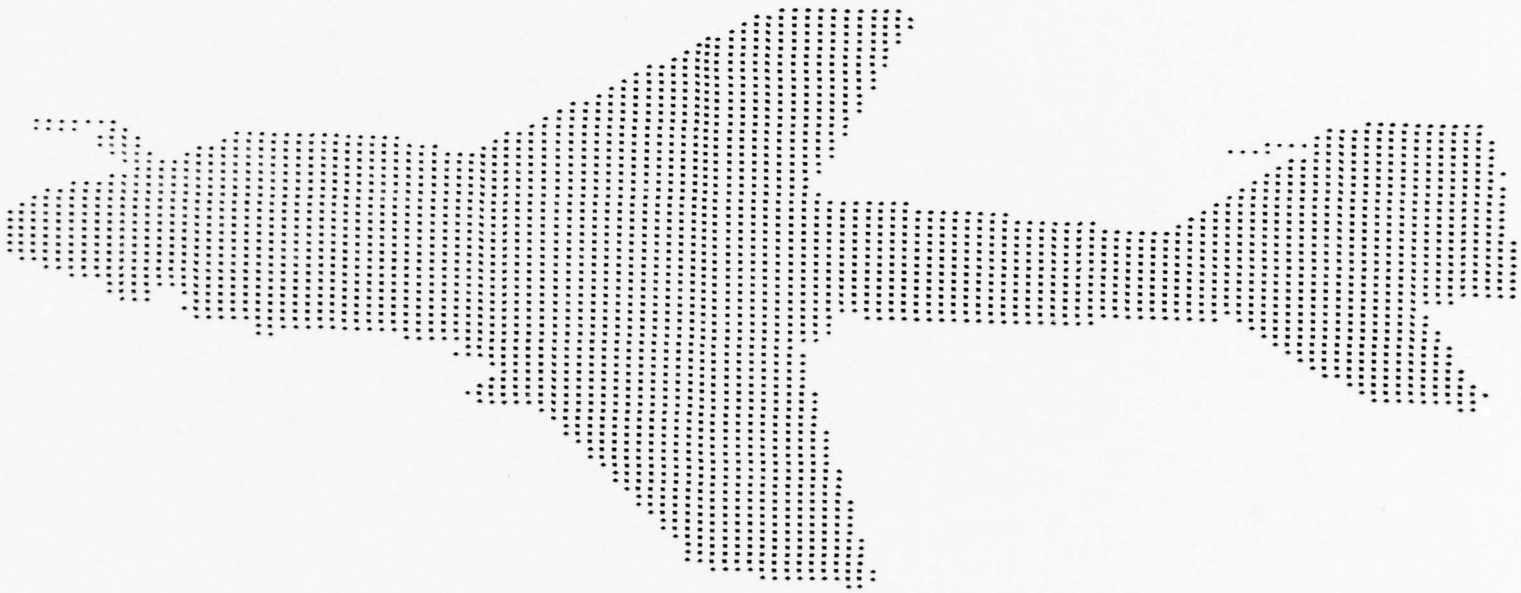

Fig. 11 Aircraft Silhouette

SILHOUETTE EXTRACTION FOR AIRCRAFT IN CLUTTERED BACKGROUND

The A-6 image used in the preceding section was clean and easy to work with because the background was clear and uncluttered. Often an aircraft will be viewed in a scene with a cluttered background consisting of clouds or ground terrain. To perform a controlled simulation to develop processing techniques for such images, the A-6 image was extracted from its background using the silhouette previously determined. Figure 12 shows the isolated A-6 (note that the extraction was not perfect since, as noted before, some of the silhouette boundary points belong to the background). The isolated aircraft was superimposed on a cloud background (digitized from the photograph in Fig. 13) to give the composite image of an aircraft flying against a cloud background (Fig. 14).

At this point the GLM boundary isolation and silhouette extraction procedures were applied with the results shown in Figs. 15 and 16. In these images, the cloud background noise was so strong that no representative silhouette could be extracted. Threshold manipulation did not help because if the threshold were raised to the point of separating the cloud background, significant points in the aircraft boundary were lost so that it was no longer closed. More complicated boundary following logic might be developed to edit out noise or fill in gaps in the boundary. A more complicated follower was tried but found inadequate; it seems the more complicated the logic of the algorithm the more likely the follower is to get lost. A more straightforward approach is to reduce the background noise in the original image before trying to extract the silhouette.

A standard means of reducing image noise is integration or time averaging. Just as differentiation tends to enhance noise,

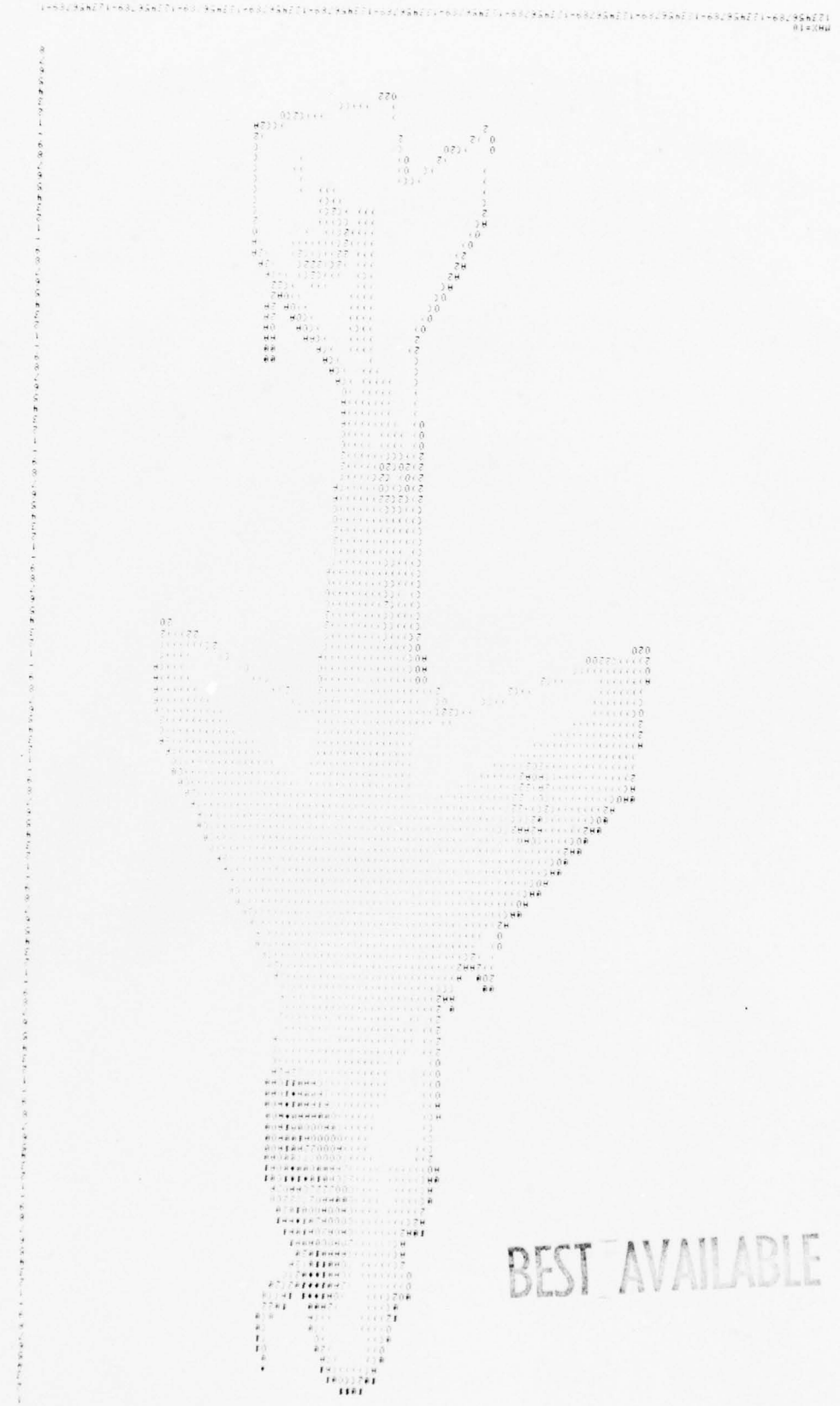

Fig. 12 Isolated A-6 Image

Fig. 13 Photograph of Cloud Background

Fig. 14 Composite Image of Aircraft and Clouds

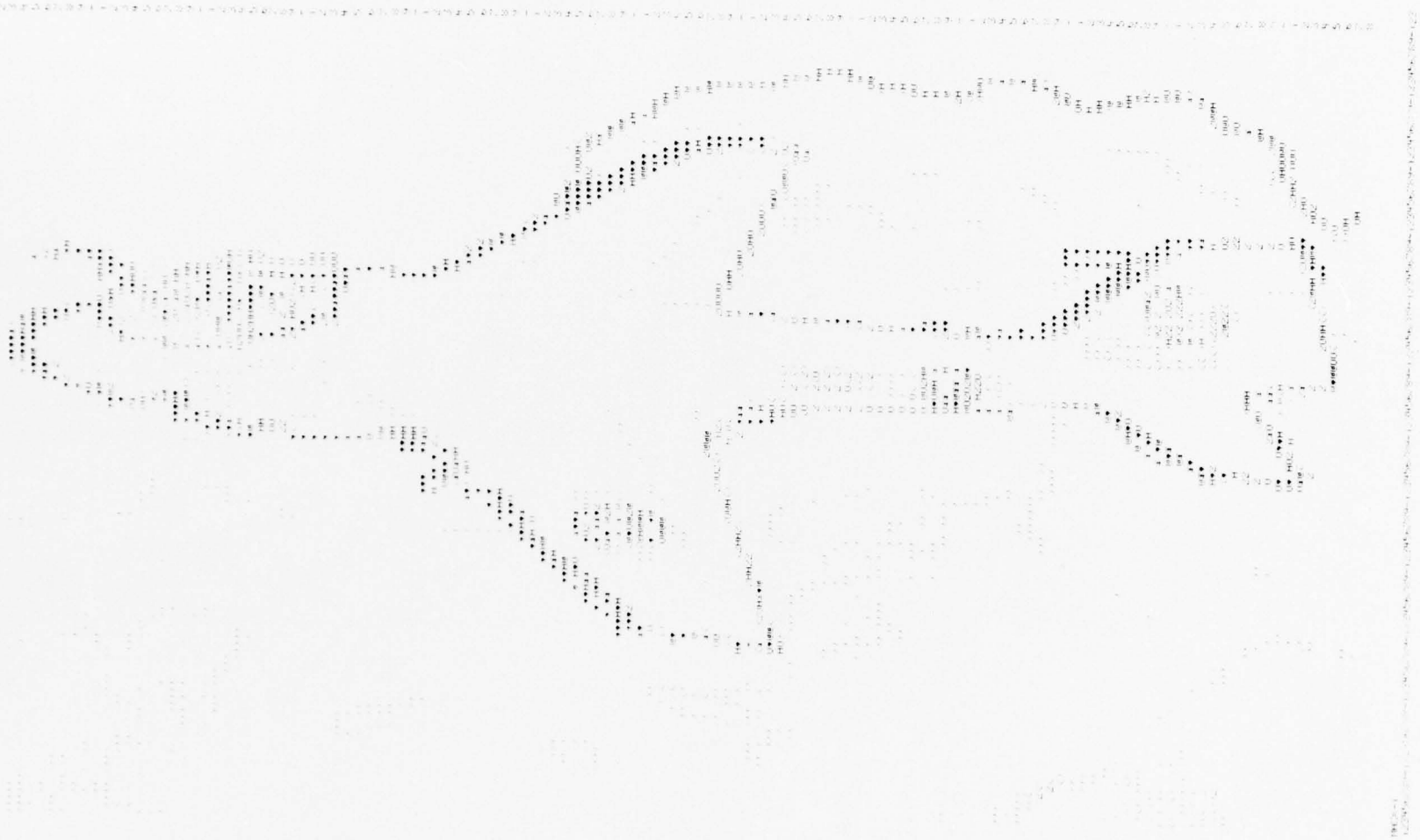

Fig. 15 Gradient Local Maxima for Aircraft and Clouds

Fig. 16 Noisy Silhouette of Aircraft and Clouds

integration tends to suppress it. Since the ultimate application of our silhouette extraction techniques will be on moving targets, we can take advantage of the availability of image information over a period of time and average successive frames of the image.

The important assumptions we must make here are that

1) the aircraft is fixed in the image frame during the interval of time over which we average (i.e., the sensor is locked onto the target)

2) the background changes to some degree during the interval (i.e., the aircraft is moving across the background)

We can relax the requirement of the first assumption somewhat if we are willing to take time to shift, scale, and rotate successive frames for maximum correlation with the running average. However, the simplest application of this procedure would be a straightforward time exposure. At a standard frame rate of 30 frames per second, 1/5 second exposure would allow 6 frames to be averaged. In any event the averaging could not be effectively applied during any time interval in which the aircraft significantly changed its aspect relative to the sensor.

To test the effectiveness of frame averaging, we composed a series of composite frames with the extracted A-6 image superimposed on the cloud image at locations separated in the horizontal direction by the minimum increment, one picture element. We then had a simulation of successive frames of an A-6 moving across a cloud background, with the A-6 fixed and the clouds moving in the frame.

The averaging technique was tested for averages of 3, 6, 12, 20, and 30 frames. No acceptable boundary was attainable for the

three frame average, but for six frames or more good boundaries and silhouettes were extracted (Figs. 17-21).

In order to give a quantitative measure of effectiveness the silhouette moment invariants were calculated for each average. For each case, the Euclidean distance between the moments of the average-image silhouette and those of the isolated A-6 served as a metric. The results are plotted in Fig. 22 where the "poor classification" and "good classification" regions were determined from averages of classification tests done in a previous study (Ref. 3).

The important result here is that after just six frames (equivalent to 1/5 of a second) an acceptable silhouette was extracted from a very noisy background. In a situation with either less noise or greater aircraft motion across the background, even fewer frames would be required.

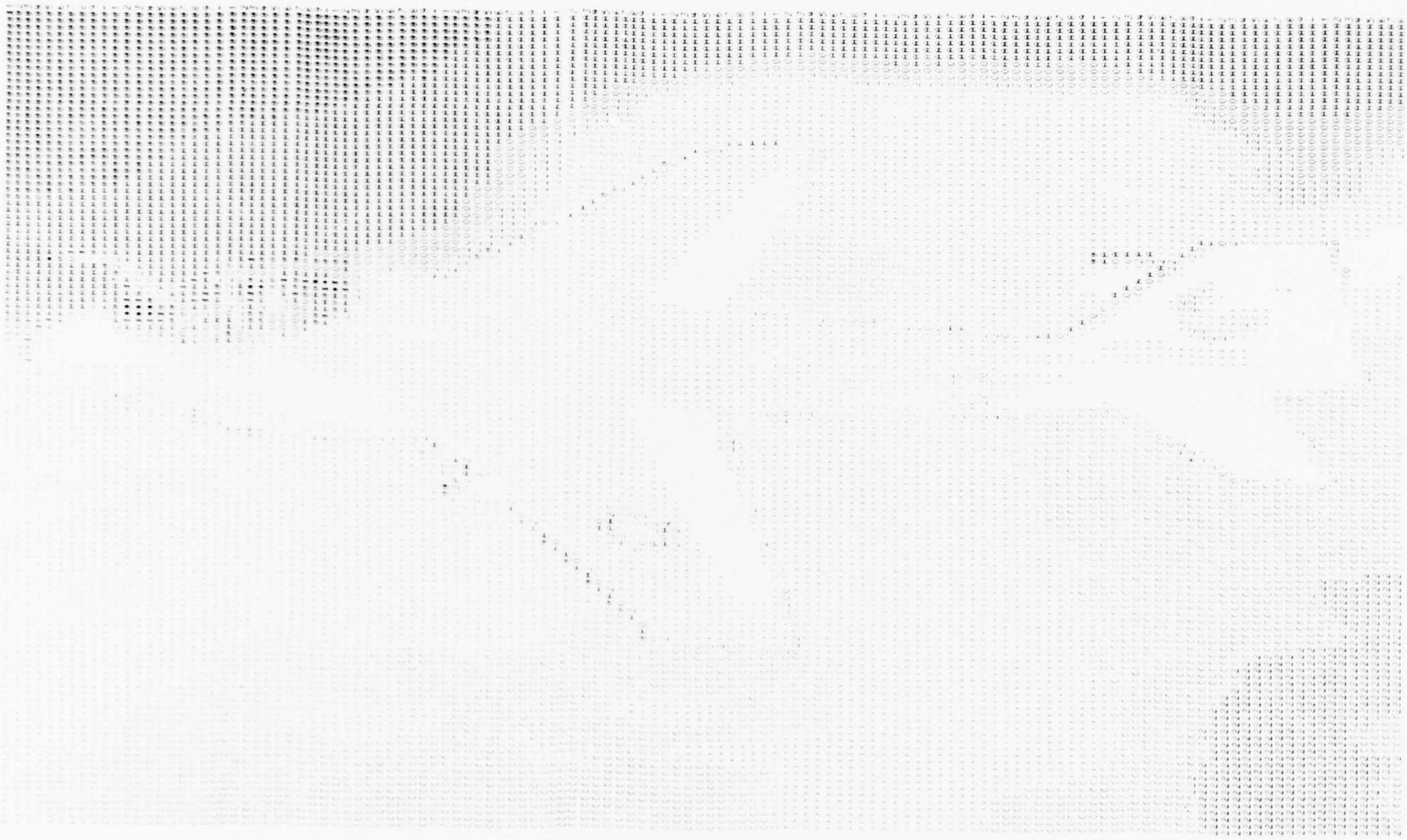

Fig. 17 Six-Frame Average of Aircraft and Clouds

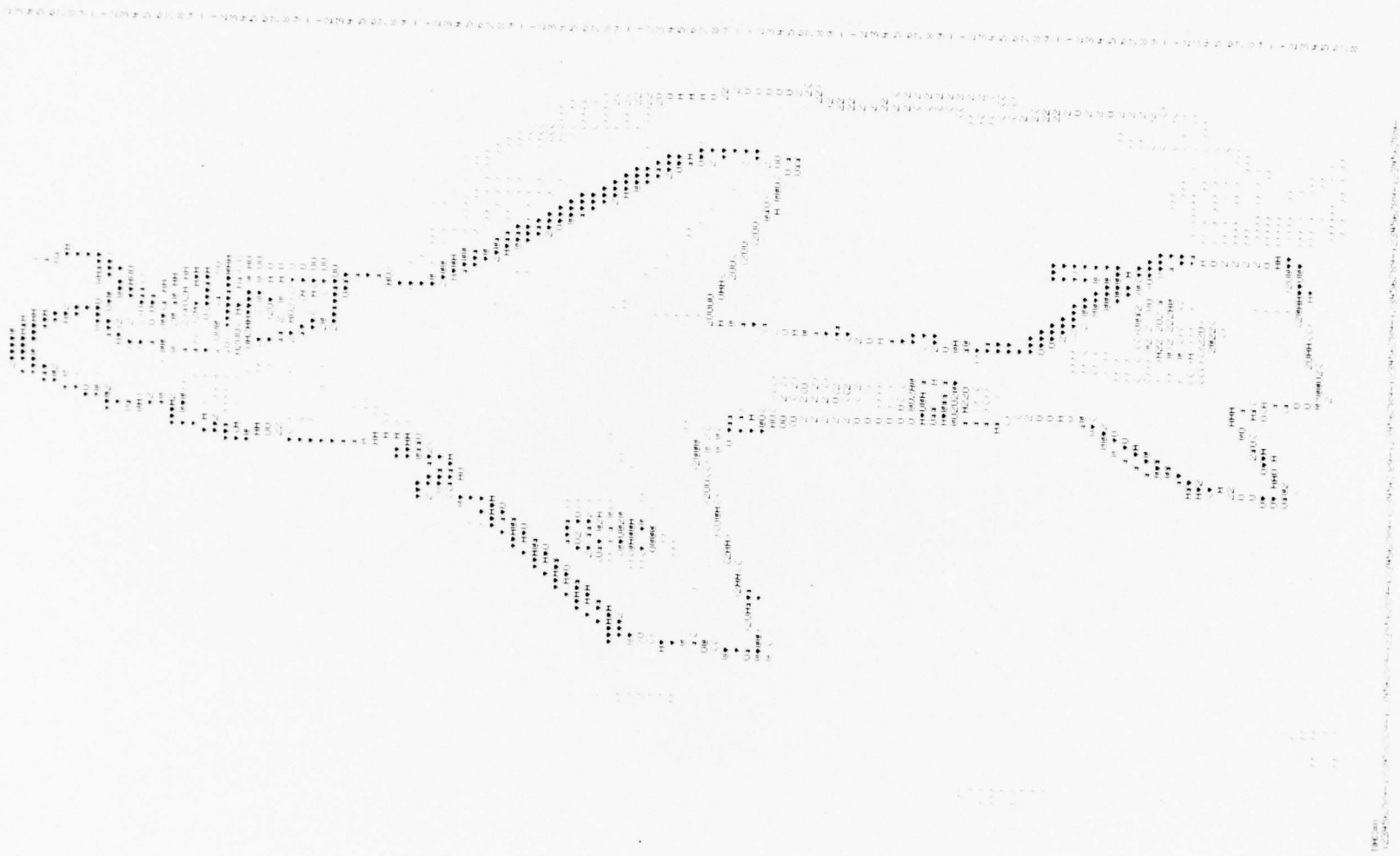

Fig. 18 Gradient Local Maxima of Six-Frame Average

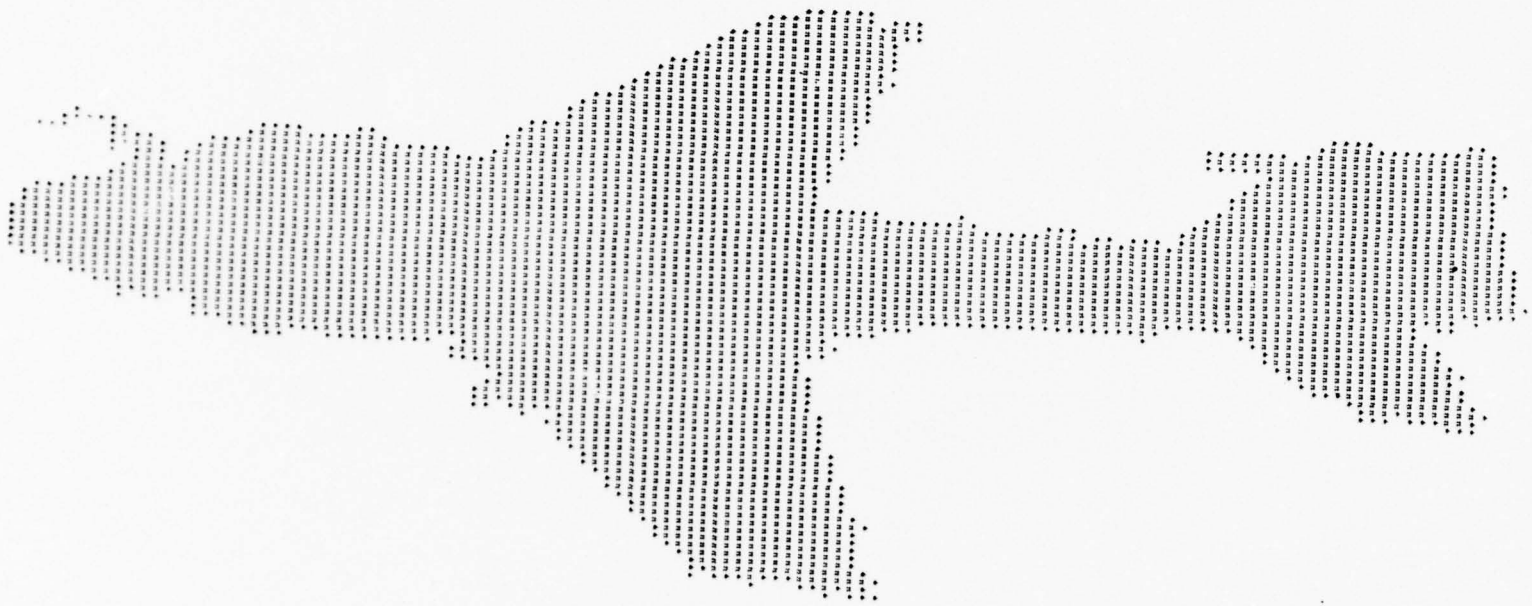

Fig. 19 Aircraft Silhouette from Six-Frame Average

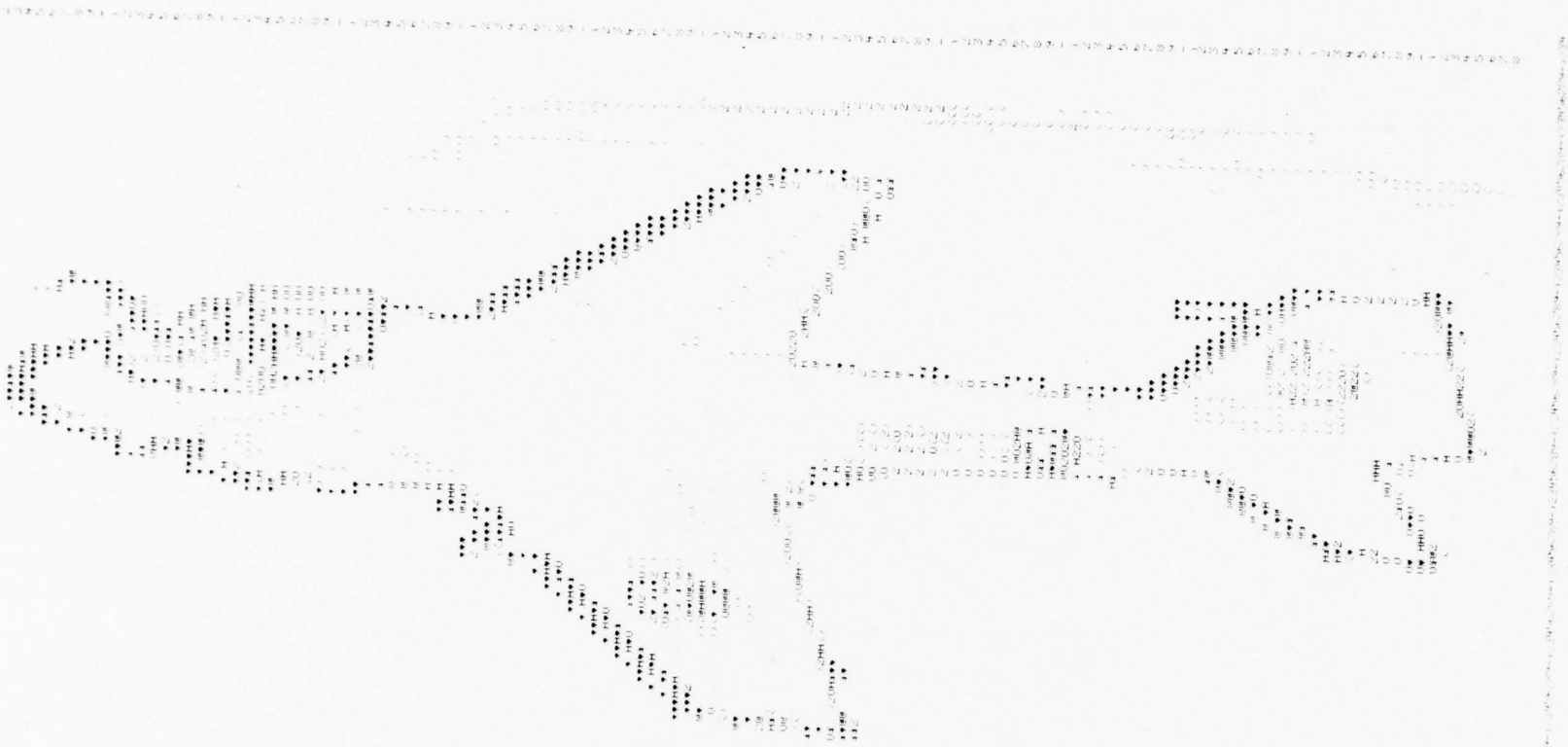

Fig. 20 Gradient Local Maxima of Twelve-Frame Average

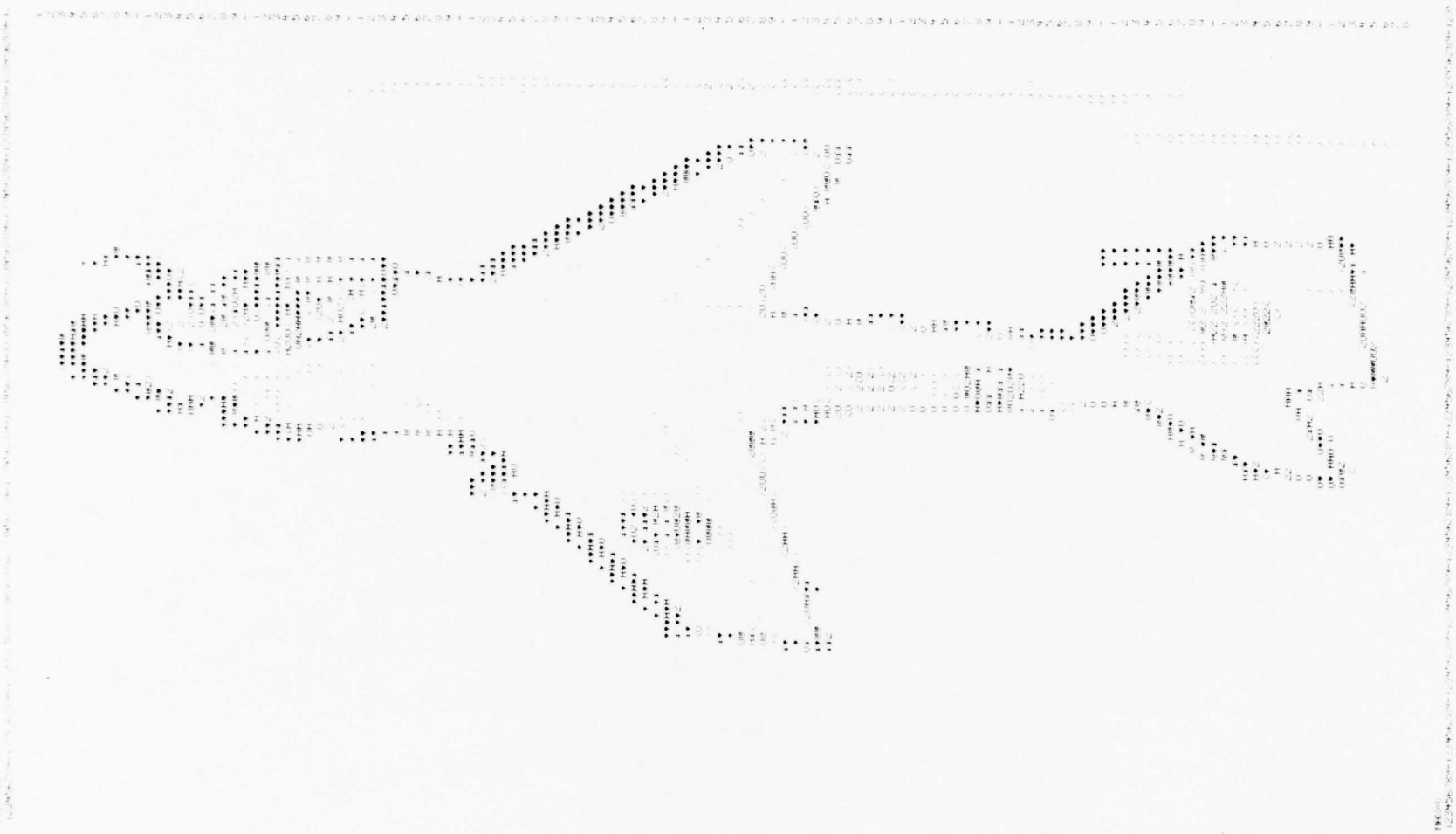

Fig. 21 Gradient Local Maxima of Twenty-Frame Average

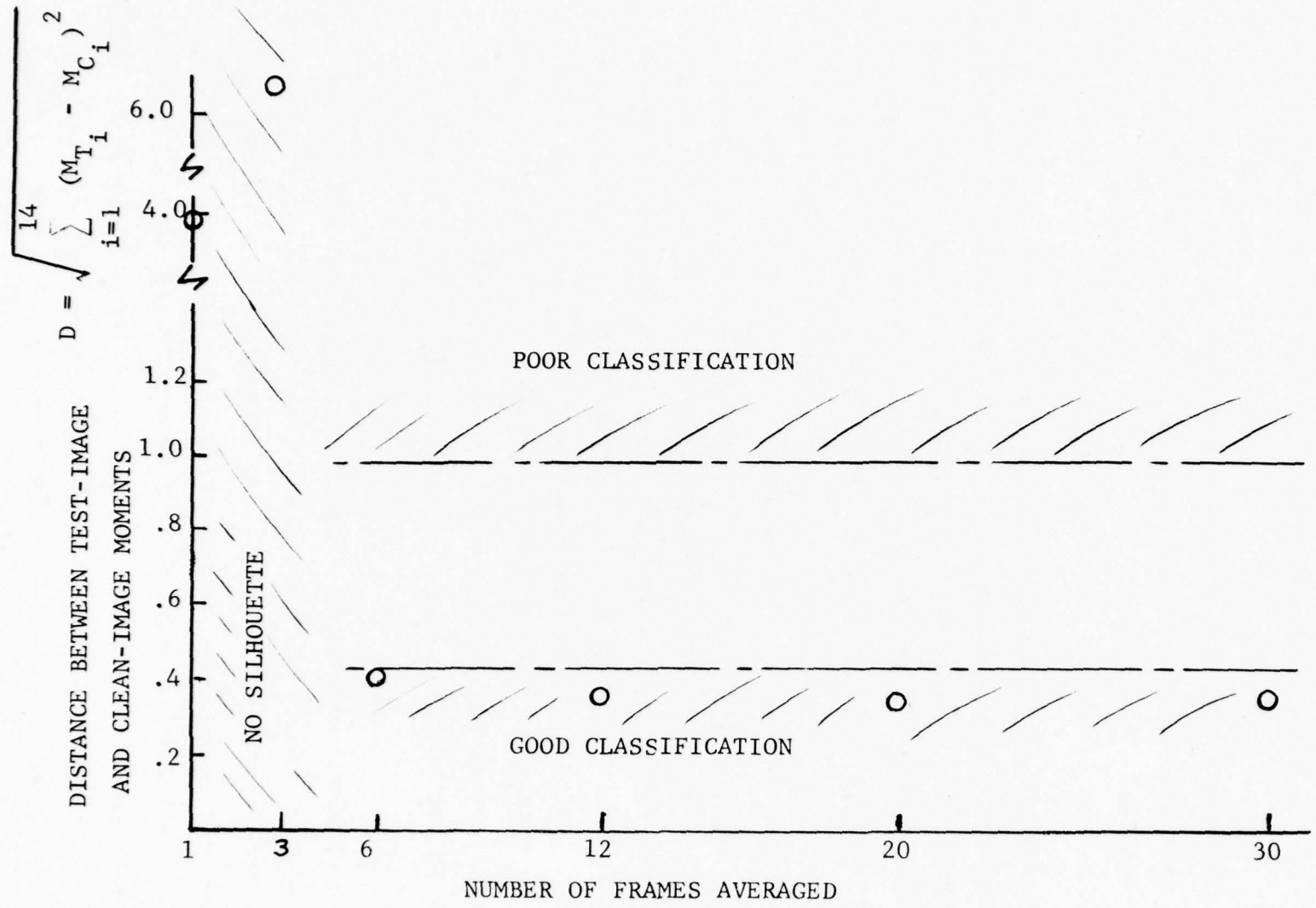

Fig. 22 Effect of Averaging Successive Frames to Suppress Noisy Background

THE EFFECTS OF SENSOR-INDUCED NOISE

Reference 3 presents a study of blurring due to sensor resolution limitations and its effect on silhouette extraction and classification. To complement this study we investigated the effect of sensor jitter on the silhouette extraction.

The effect of jitter was simulated by applying an 11 x 11 pixel window to the clean image of the A-6 flying before a clear background. The weighting of the window was a truncated gaussian distribution centered at the center pixel and having a variable standard deviation which was used as a metric to quantify the jitter. The metric for quality of the extracted silhouette was the Euclidean distance between moments of the jittered image and those of the unjittered image. The results are shown in Fig. 23. The moment distance leaves the good classification region at a jitter standard deviation (SD) of about .85 and enters the poor classification region at an SD of about 1.3. At a distance of 100 miles, with one pixel representing 0.5 feet in the A-6 image these SD values correspond to angular values of 1.7 μ and 2.6 μ radians, respectively. These values were compared to the average results of the blurring study in Ref. 3 and agreed within a factor of 2.

The combined effects of jitter and background clutter were simulated by actually shifting each of the six composite A-6/cloud images and averaging. The shift was determined by a random number generator with a gaussian distribution of predetermined SD. Since shifting could only be accomplished on a quantized level, however, the simulation was somewhat crude. A shift distribution with SD up to 0.6 allowed successful silhouette extraction with moment distances in the good classification range.

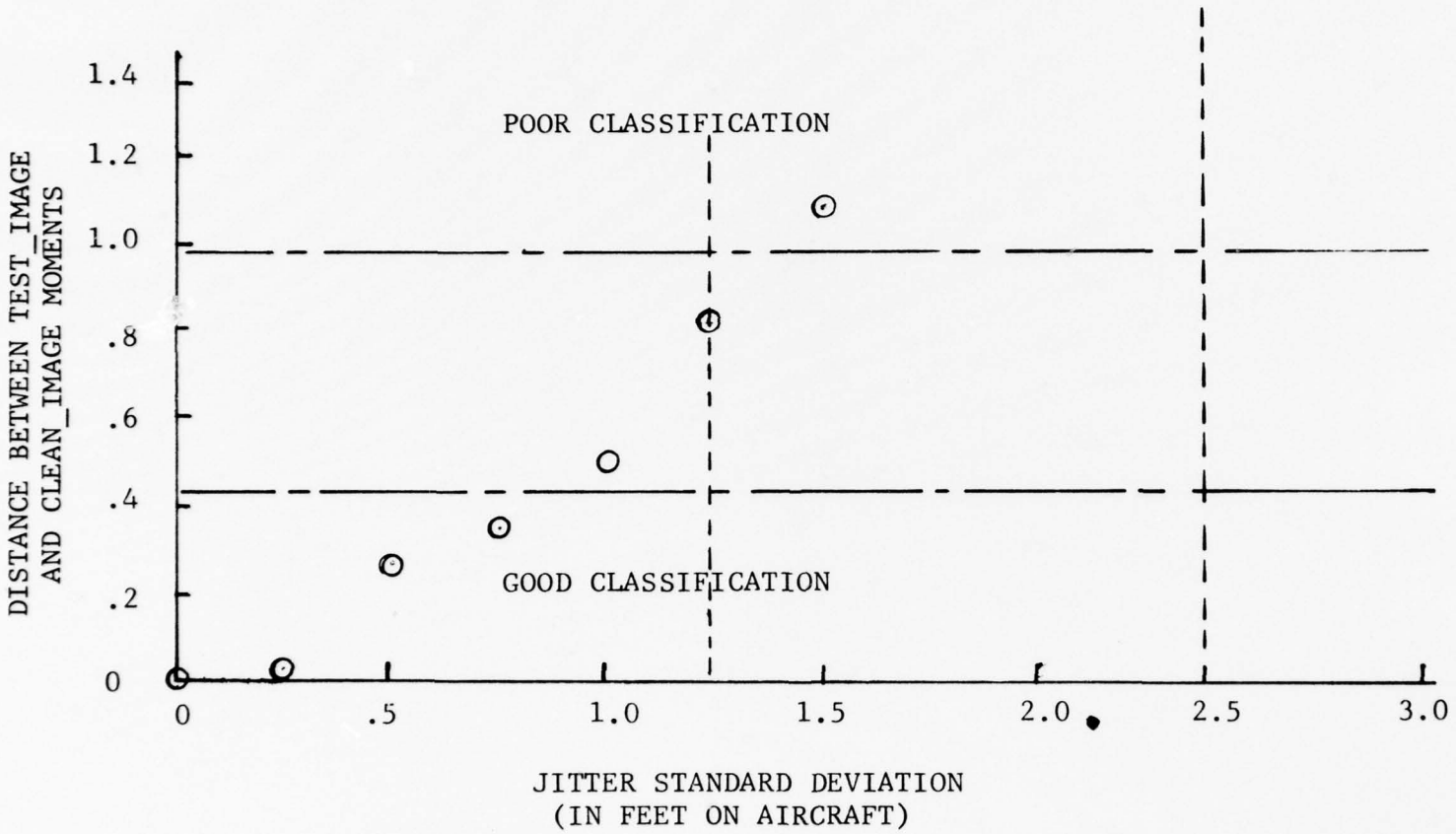

Fig. 23 Effect of Gaussian Jitter

The effect of jitter on classification indicates the importance of the sensor being locked onto the target.

SILHOUETTE EXTRACTION FROM FLIR IMAGES

The feasibility of applying our silhouette extraction techniques to other sensors was tested on three FLIR images of an F-14 taken from near-sequential frames of a video tape (Figs. 24 and 25). To reduce noise (Fig. 26) the three images were averaged (Fig. 27) and the GLM technique applied to obtain the silhouette (Figs. 28 and 29). Because the average image had reasonably distinct intensity levels for the aircraft and background, the "true" silhouette was obtained by thresholding the intensity (Fig. 30). The GLM derived and true silhouette moments agreed within the good classification region.

Fig. 24 Three FLIR Images (Sheet 1 of 3)

Fig. 24 Three FLIR Images (Sheet 2 of 3)

Fig. 24 Three FLIR Images (Sheet 3 of 3)

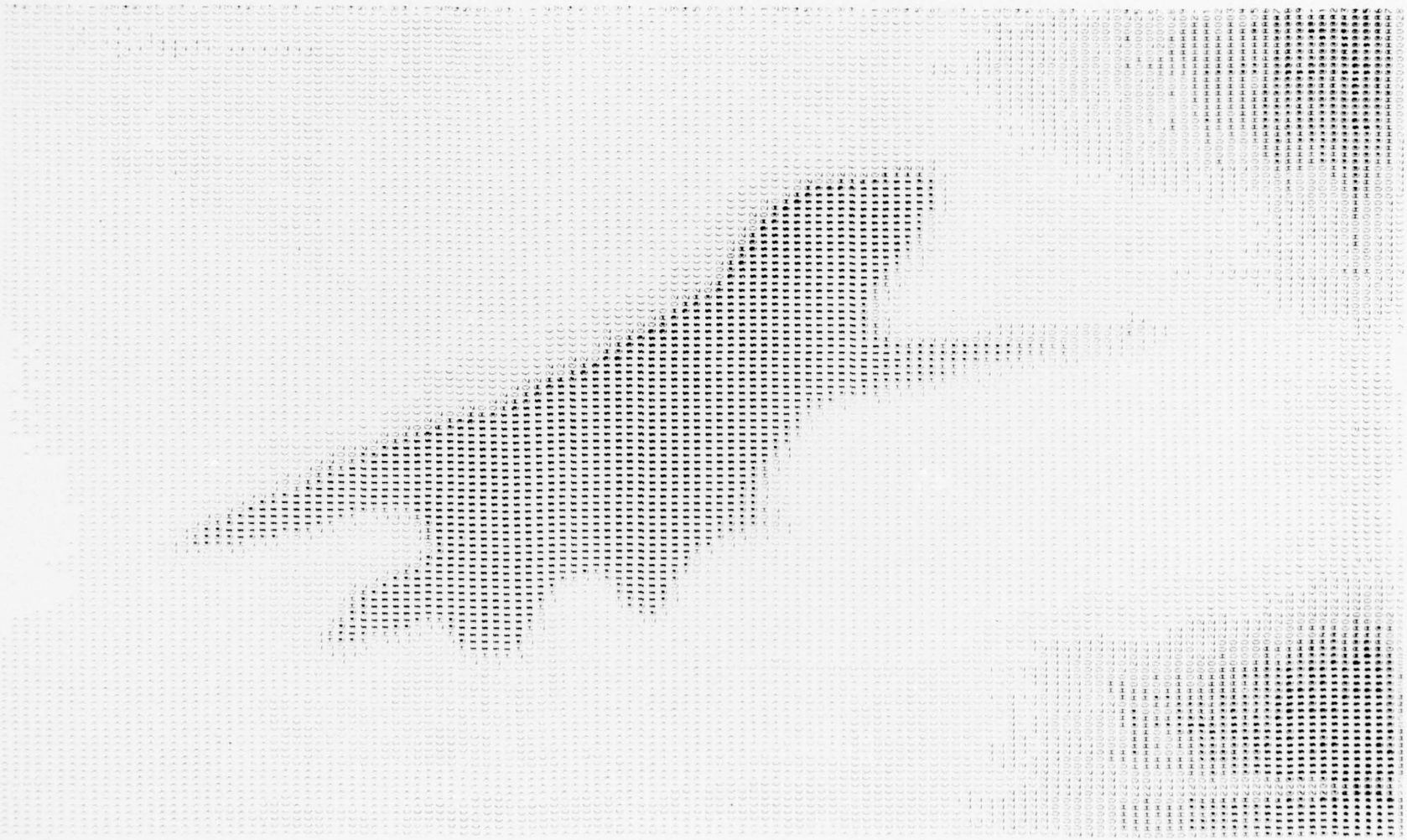

Fig. 25 Digitized FLIR Images (Sheet 1 of 3)

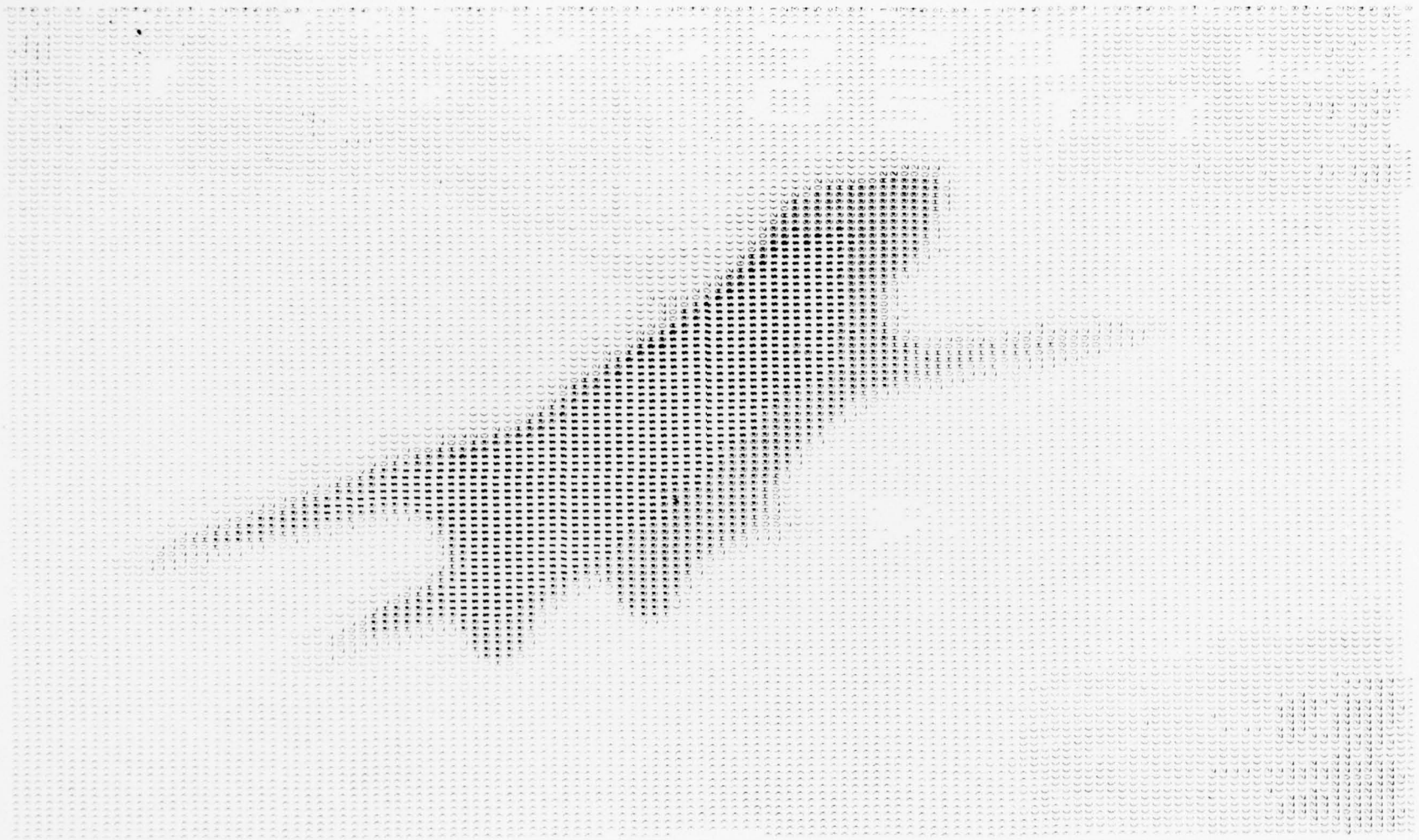

Fig. 25 Digitized FLIR Images (Sheet 2 of 3)

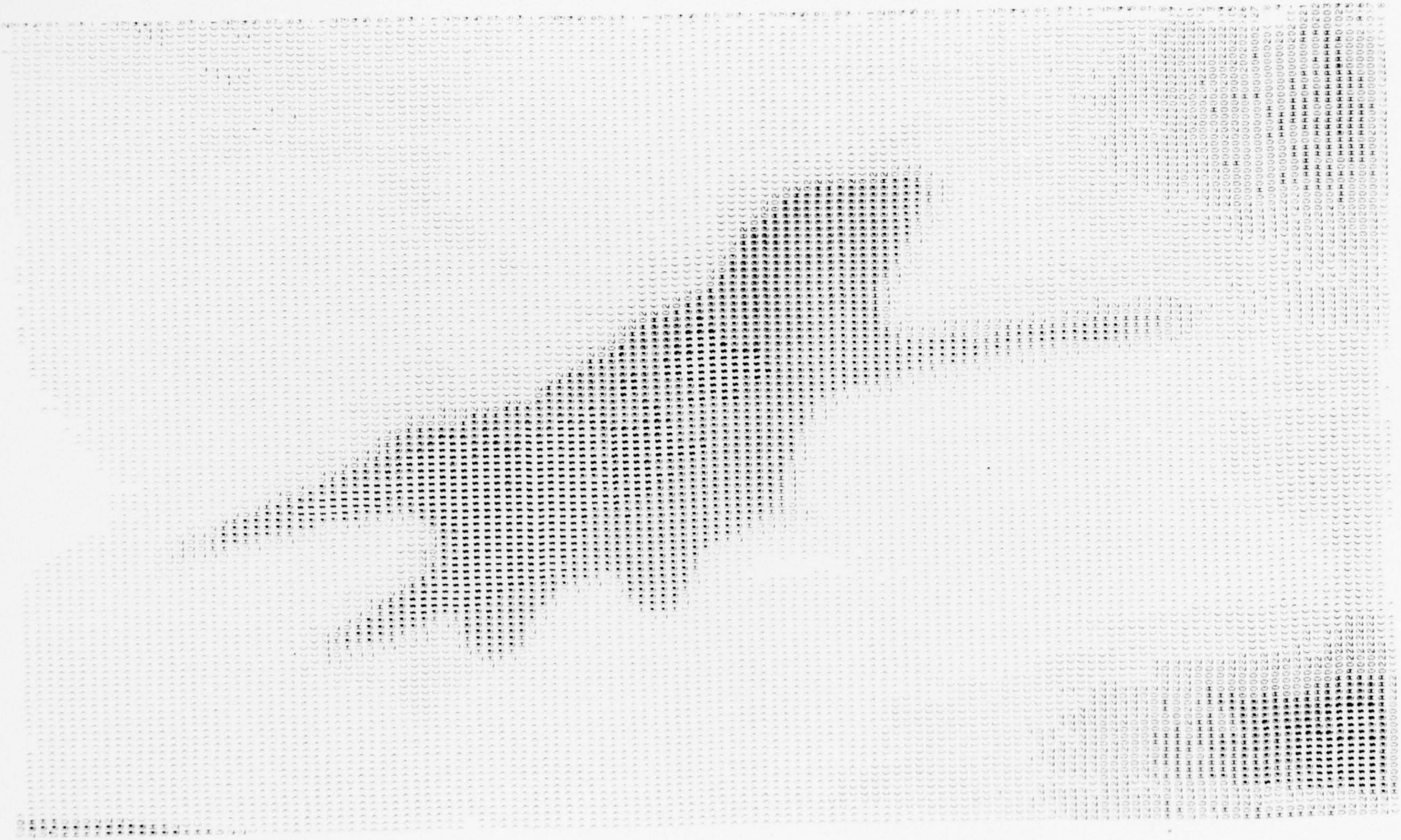

Fig. 25 Digitized FLIR Images (Sheet 3 of 3)

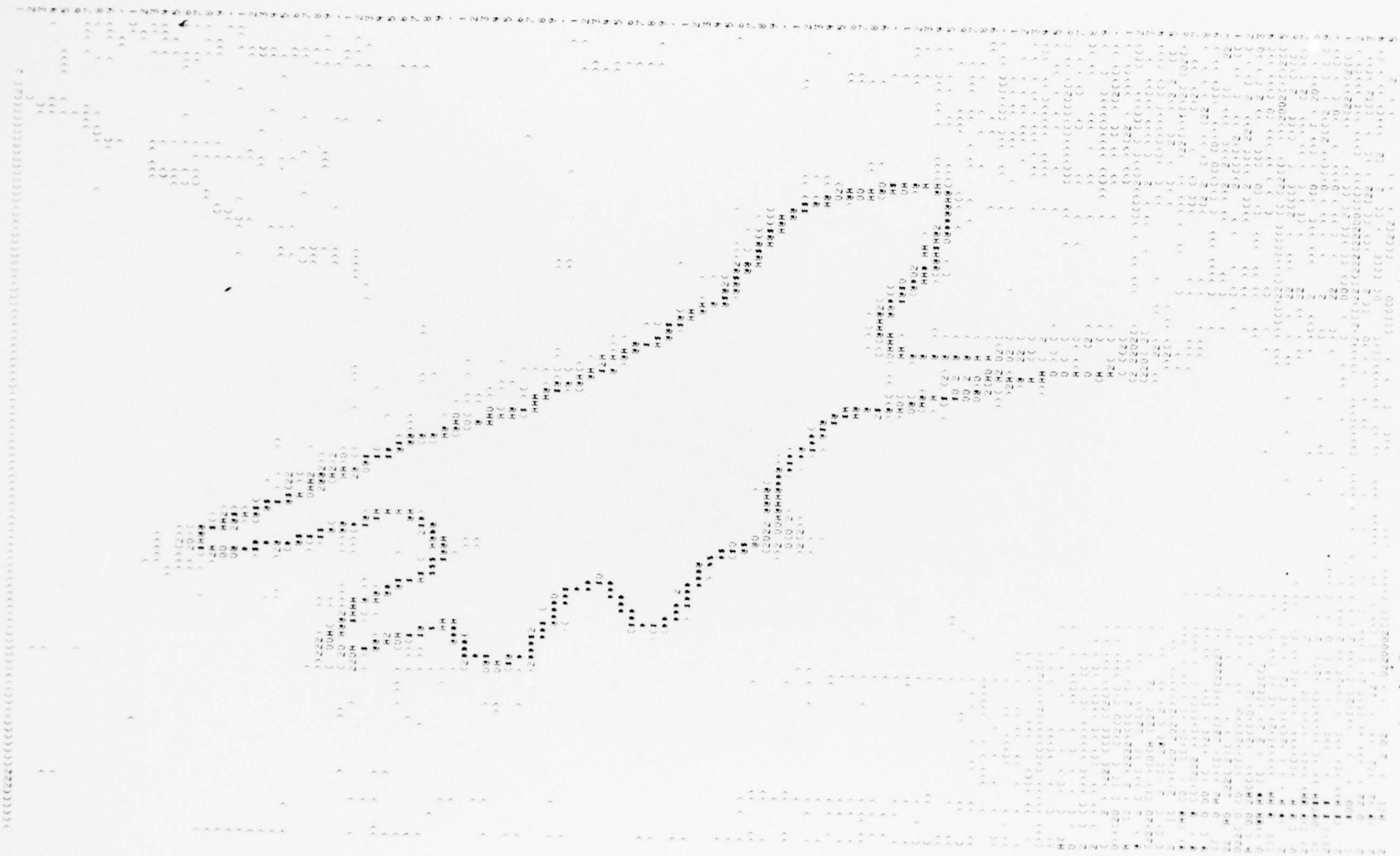

Fig. 26 Gradient Local Maxima of First FLIR Image

Fig. 27 Average of Three FLIR Images

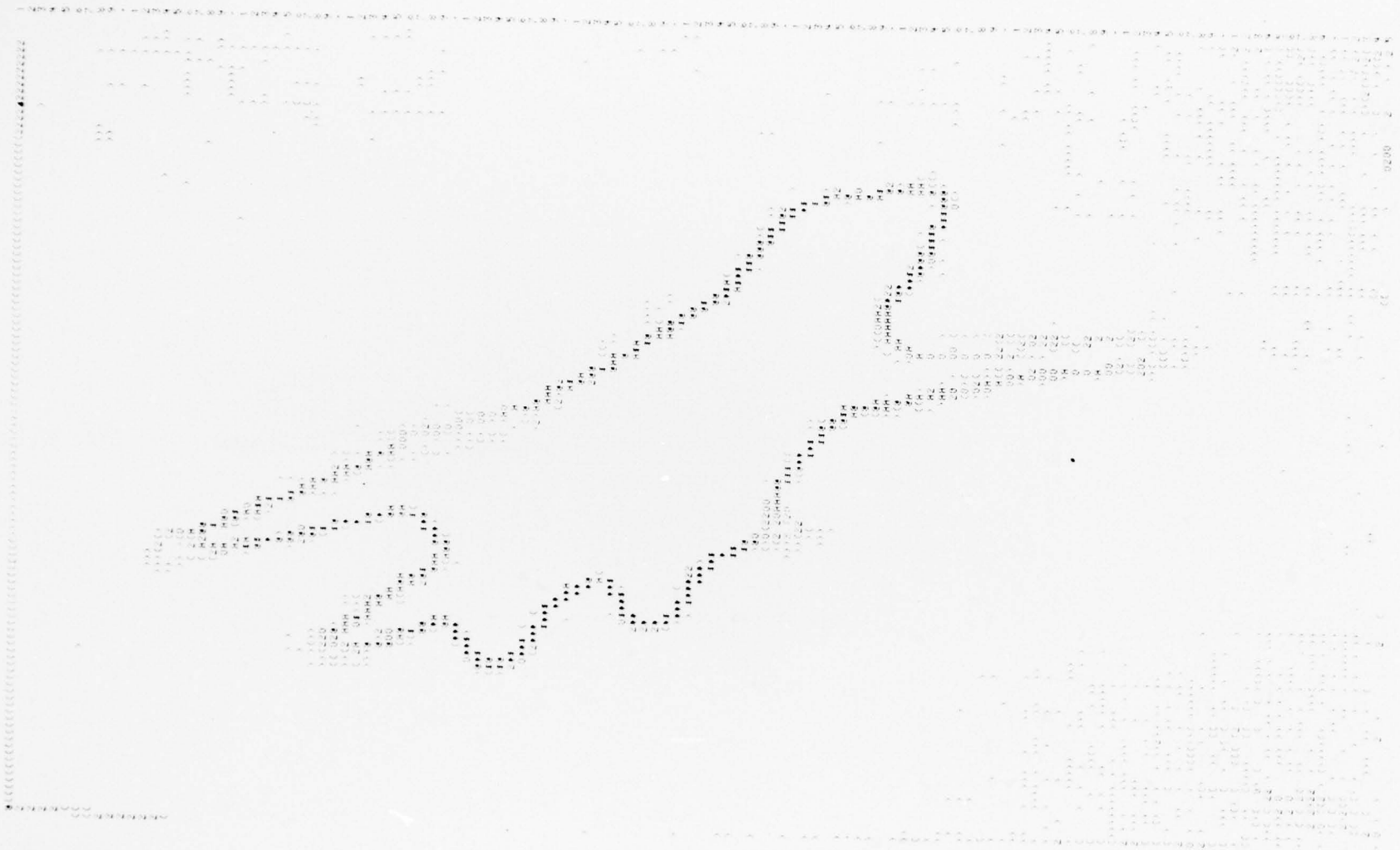

Fig. 28 Gradient Local Maxima of Average FLIR Image

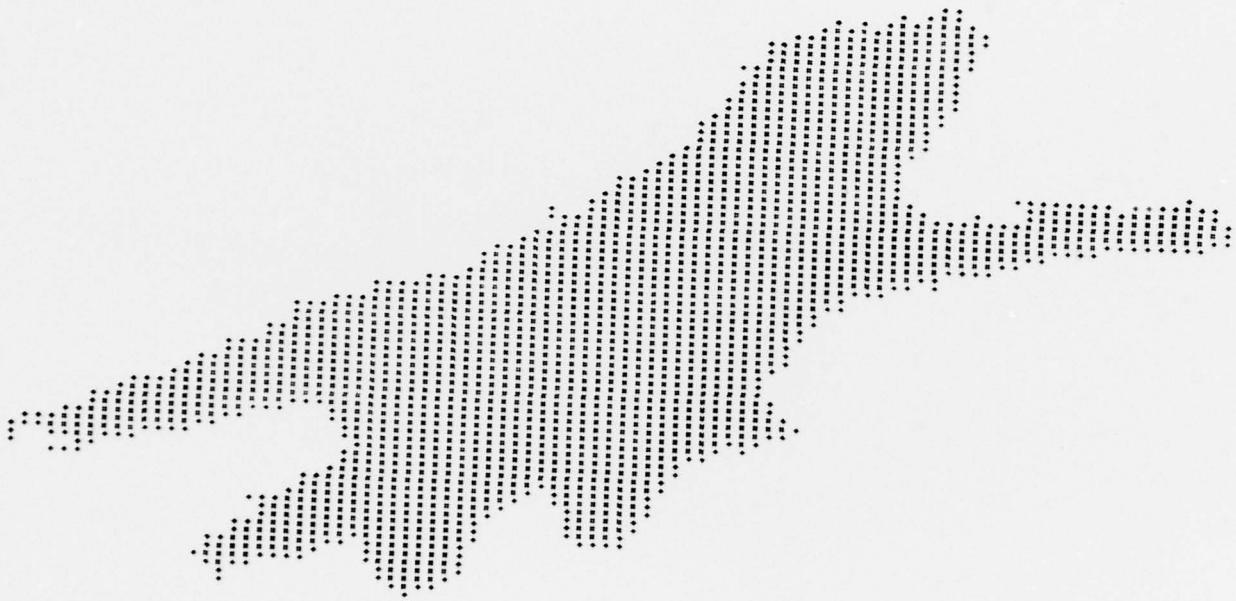

Fig. 29 GLM-Derived Silhouette of Average FLIR Image

Fig. 30 Intensity-Derived Silhouette of Average FLIR Image

CONCLUSIONS

The digital techniques developed in this study have been shown to possess the potential for extending Dudani's moment invariant classification method to real world aircraft images. Aircraft silhouettes can be effectively extracted from full gray scale images by the gradient local maxima method. Even images with considerable background noise and sensor induced noise can be effectively processed. In addition, the techniques have been demonstrated successfully on FLIR imagery.

REFERENCES

1. Dudani, S. A., "An Experimental Study of Moment Methods for Automatic Identification of Three Dimensional Objects from Television Images," Doctoral Dissertation, Department of Electrical Engineering, Ohio State University, August 1973.

2. Fram, J. R. and Deutsch, E. S., "On the Quantitative Evaluation of Edge Detection Schemes and Their Comparison with Human Performance," IEEE Transactions on Computers, Vol. C-24, No. 6, pp. 616-627, June 1975.

3. Mendelsohn, J., Gardner, G., and Wohlers, M., "The Effect of Blurring on Aircraft Classification by the Moment Method," Grumman Research Department Memorandum RM-620, June 1976.